

# $\Delta$ -model correction of Foundation Model based on the models own understanding

Mads-Peter Verner Christiansen and Bjørk Hammer\*

*Center for Interstellar Catalysis, Department of Physics and Astronomy,  
Aarhus University, DK-8000 Aarhus C, Denmark*

(Dated: March 3, 2025)

Foundation models of interatomic potentials, so called universal potentials, may require fine-tuning or residual corrections when applied to specific subclasses of materials. In the present work, we demonstrate how such augmentation can be accomplished via  $\Delta$ -learning based on the representation already embedded in the universal potentials. The  $\Delta$ -model introduced is a Gaussian Process Regression (GPR) model and various types of aggregation (global, species-separated, and atomic) of the representation vector are discussed. Employing a specific universal potential, CHGNet [Deng *et al.*, Nat. Mach. Intell. **5**, 1031 (2023)], in a global structure optimization setting, we find that it correctly describes the energetics of the "8" Cu oxide, which is an ultra-thin oxide film on Cu(111). The universal potential model even predicts a more favorable structure compared to that discussed in recent DFT-based literature. Moving to sulfur adatom overlayers on Cu(111), Ag(111), and Au(111) the CHGNet model, however, requires corrections. We demonstrate that these are efficiently provided via the GPR-based  $\Delta$ -model formulated on the CHGNet's own internal atomic embedding representation. The need for corrections is tracked to the scarcity of metal-sulfur atomic environments in the materials project database that CHGNet is trained on leading to an overreliance on sulfur-sulfur atomic environments. Other universal potentials trained on the same data, MACE-MP0, SevenNet-0, and ORB-v2-only-MPtrj show similar behavior, but with varying degrees of error, demonstrating the general need for augmentation schemes for universal potential models.

## I. INTRODUCTION

Quantum mechanical calculations of material properties have been a corner stone of material science for the past several decades. This encompasses e.g. the prediction or theoretical explanation of phase diagrams of solids or surfaces. In recent years the advancement of machine learning (ML) techniques as a set of tools to reduce the computational expense of such studies has become widespread [1].

Perhaps the most common use of ML is that of replacing expensive first-principles calculations of total energies with orders of magnitude faster machine-learning interatomic potentials (MLIPs). Early works in this area included Behler-Parinello neural networks and the Gaussian Approximation Potentials of Bartok *et. al* [2, 3]. Since then many advances have been made improving the accuracy and data efficiency of these potentials [4–17]. With these improvements many tasks in computational material science have benefitted from the efficiency they offer, however often demanding the construction of a task specific dataset, thus still requiring expensive ab-initio calculations.

Recently datasets containing ab-initio properties of atomic configurations covering vast regions of chemical space have become available [18–20]. These data sets have enabled the creation of the atomistic equivalent of foundation models – universal potentials. One such dataset is the Materials Project Trajectory (MPtrj) containing among others energies and forces for some  $\sim 1.6$  million structures extracted from the Materials Project.

Several MLIPs have been trained on this dataset including CHGNet, MACE-MP0, SevenNet-0, and ORB-v2-only-MPtrj [18, 21–23].

One area that will benefit from these potentials is that establishing which phases of a material are stable under physically relevant conditions. One strategy in this domain is global structure optimization, finding the most energetically, in terms of total energy, favorable geometries of an atomic system followed by a thermodynamic analysis to identify the phases with the lowest Gibbs free energy. The optimization step requires exploration of the potential energy surface, a task that has received much research interest in order to provide effective algorithms [24–29]

The construction of accurate phase diagrams depends critically on the accuracy of the underlying total energy description. In our recent work on describing the global optimal structure of silicate clusters and ultra-thin oxide films on Ag(111) with CHGNet, it was found necessary to augment the CHGNet model with  $\Delta$ -learning in order to get the correct order of stability of low-lying structures [30]. In that work, the  $\Delta$ -model was built on a representation involving the SOAP descriptor for each atom. In the present work, we introduce the necessary formalism for eliminating the need of such a descriptor and instead use the internal representation of the atoms in the CHGNet when constructing the  $\Delta$ -model. Employing the method in a global optimization setting, we find the resulting corrections for ultra-thin oxide films on Cu(111)-*c*( $8 \times 4$ ) to be small. The search results in an oxide film structure that represents a reinterpretation of the experimentally found structure. This result clearly testifies to a high quality of a foundation model such as CHGNet.

In contrast, for sulfur ad-atom layers on Cu(111),

---

\* hammer@phys.au.dk

Ag(111), and Au(111) we find that the correction terms resulting from the delta model are more critical, in particular for Ag(111) and Au(111). By analyzing the similarity of local atomic environments in the sulfur ad-layer systems and in the training database for CHGNet, we trace the origin of the low accuracy in these systems to the lack of relevant Ag-S and Au-S local environments in the training data.

The paper is structured as follows: First we introduce the methodologies employed, this includes an account of the descriptor we employ which has been extracted from CHGNet, the Gaussian Process Regression scheme that we use, and a summary of the global optimization (GO) algorithm used for structural searches. Next, we present the computed phase diagrams for O/Cu(111) and S/Au(111), showing the need for corrections in the latter case. The paper proceeds by comparing the CHGNet behavior for a specific S-coverage on Cu(111), Ag(111), and Au(111) and relates that to the occurrence of relevant structures in the MPtrj dataset thereby shedding light on why CHGNet gets the relatively simple sulfur overlayer structure so wrong when it is capable of predicting a previously undiscovered phase of the copper oxide. The paper ends by identifying that the issues for the sulfur ad-layers pertains to other foundation models, MACE-MP0, SevenNet-0, and ORB-v2-only-MPtrj, that have all been trained on the same dataset as CHGNet.

## II. METHODOLOGY

### A. Description of Atomic Environments

The development and success of machine learning tools in computational materials science has been driven by iterative improvements to the description of environments. The field initially relied on handcrafted descriptors, such as Behler-Parinello symmetry functions [31], the Valle-Oganov fingerprint [32] or the Smooth Overlap of Atomic Positions (SOAP) formalism [33]. Since then neural networks such as SchNet that are capable of learning useful representations directly from Cartesian coordinates have become widespread [8, 34, 35].

Recently such neural networks have been trained on large datasets resulting in so-called universal potentials – the atomistic equivalent of a foundation model. One such foundation model is CHGNet, which has been trained on the MPtrj dataset [18]. CHGNet is a graph neural network where message-passing operations are used to iteratively update the representation of each atom with information from its surrounding neighbors. The layout of CHGNet is shown schematically in the green box of Fig. 1. A prediction from CHGNet, and likewise for the majority of other graph based MLIPs, is calculated by first updating the atomic representations with message-passing and then passing these refined descriptors to a prediction head, that transforms and aggregates the descriptors in order to produce a prediction. Typi-

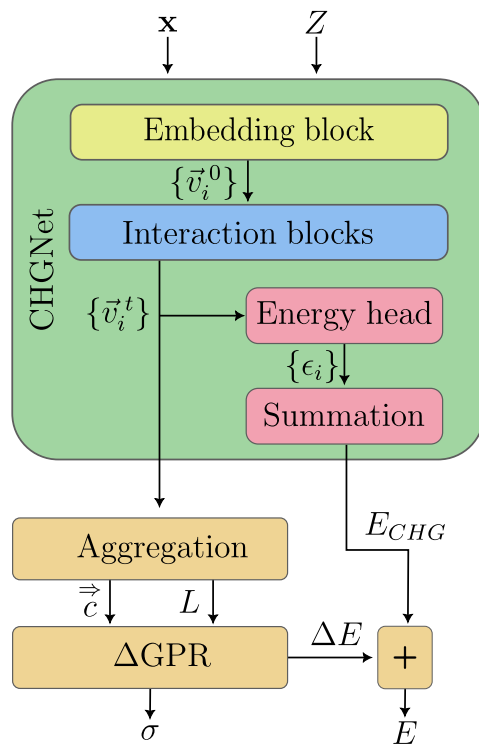


FIG. 1. Illustration of our use of CHGNet, including a summarized version of CHGNet and our additional  $\Delta$ -model using the CHGNet atomic representations.

cally, an energy prediction is made by transforming the high-dimensional descriptors to a scalar for each atom and summing these together. We will use  $\vec{v}_i$  to denote representations of atomic environments extracted from CHGNet. These are 64 dimensional vectors one for each atom in an atomic configuration. These descriptors may be extracted and used for other tasks, such as  $\Delta$ -learning as shown schematically with the brown boxes in Fig. 1.

For a full description of the architecture of CHGNet, we refer to Figure 1 of the original publication Ref. [18]. For the present purposes, it serves to summarize it as:

1. Initialize relevant properties for the message-passing, including initial descriptors,  $\vec{v}_i^0$ .
2. Apply message-passing interaction blocks  $t - 1$  times resulting in descriptors  $\vec{v}_i^{t-1}$  for each atom  $i$ .
3. Predict magnetic moments using vectors  $\vec{v}_i^{t-1}$ .
4. Apply one more message-passing block to compute vectors  $\vec{v}_i^t$ .
5. Predict atomic energies  $\epsilon_i$  using the vectors  $\vec{v}_i^t$ .
6. Sum local energies to predict total energy  $E = \sum_i \epsilon_i$ .

CHGNet consists of a representation part, that uses message-passing to construct descriptors of atomic envi-

ronments, steps 1 through 4, and a fully-connected neural network that converts each atomic descriptor to an atomic energy and the atomic energies are summed to compute the total energy, steps 5 and 6. The individual atomic descriptors are 64-dimensional vectors. We use the final atomic descriptors  $\vec{v}_i^t$  as the basis for a  $\Delta$ -model described in the next section.

## B. Additive Gaussian Process Regression

We follow our recent proposal [30] and employ a Gaussian Process Regression (GPR) model in a  $\Delta$ -learning context for correcting the universal potential in regions where it makes incorrect predictions. However, in this work, we introduce a different formalism that ties more closely together with the neural network.

Customarily the predicted mean of a GPR is given by

$$m(R) = k(R, \mathbf{X})[K(\mathbf{X}, \mathbf{X}) + \sigma_n^2 \mathbf{I}]^{-1} y. \quad (1)$$

Where  $R$  is the representation of a query object,  $\mathbf{X}$  are representations of the training data, typically a matrix where each row is a feature vector but can more generally be considered as a set of representations of the training examples. Each training example comes with a corresponding target  $y$  and  $\sigma_n^2$  is the variance of the assumed noise and  $\mathbf{I}$  is the identity matrix. The representation  $R$  may describe the full object through descriptors of parts of the object. To facilitate this, an additive kernel may be defined:

$$K_{\text{add}}(R_v, R_w) = \sum_i^{n_v} \sum_j^{n_w} L_i^v L_j^w K(\vec{v}_i, \vec{w}_j). \quad (2)$$

Here  $R_v$ , the representation of object  $v$ , which consists of  $(\vec{c}_v, L_v)$  where  $\vec{c}_v = [\vec{v}_1, \vec{v}_2, \dots, \vec{v}_{n_v}]$  is a collection of vectors describing  $v$  and  $L_i^v$  is the number of contributions associated with each vector  $\vec{v}_i$  – likewise  $R_w = (\vec{c}_w, L_w)$ . This type of kernel can compare two objects represented by a different number of vectors and with a different number of contributions. If  $\vec{c}_v = [\vec{v}_1]$ ,  $\vec{c}_w = [\vec{w}_1]$  and  $L_1^v = L_1^w = 1$  it is evident that the original kernel  $K(\vec{v}_1, \vec{w}_1)$  is recovered. This introduces the additional property  $L$ , which we may also use to write the additive kernel in matrix form

$$K_{\text{add}}(R_v, R_w) = L_v K(\vec{c}_v, \vec{c}_w) L_w^T \quad (3)$$

With this expression we can write Eq. (1) with an additive kernel as,

$$m(R_v) = L_v k(\vec{c}_v, \mathbf{X}) L_X^T [L_X K(\mathbf{X}, \mathbf{X}) L_X^T + \sigma_n^2 \mathbf{I}]^{-1} y. \quad (4)$$

For the task of learning total energies of atomic configurations starting from vectors describing the environment of individual atoms this leaves us with several options of how to construct the representations  $R$ . This is essentially a choice of an aggregation procedure

- Global aggregation:  $\vec{c} = [\frac{1}{N} \sum_i^N \vec{v}_i]$  and  $L = [N]$  or  $L = [1]$ .
- Atomic aggregation:  $\vec{c} = [v_1, \dots, v_N]$  and  $L = [1, \dots, 1]$
- Species aggregation:  $\vec{c} = [c_1, c_2, \dots, c_M]$  where  $c_m = \frac{1}{N_m} \sum_i^N \vec{v}_i \cdot \delta(\mathcal{Z}_m, Z_i)$  and  $L = [N_1, N_2, \dots, N_M]$

Where  $N$  is the total number of atoms in a configuration,  $\vec{v}_i$  are atomic descriptors,  $M$  is the number of different species,  $N_m$  is the number of atoms of species  $\mathcal{Z}_m$ ,  $Z_i$  is the species of atom  $i$  and  $\delta$  is the Kronecker delta function. These aggregation procedures are depicted in Figure 2. With a global aggregation scheme the model learns the total property directly and by using  $L = [N]$  it is capable of learning from data involving different amounts of atoms (unlike the situation if  $L = [1]$  is chosen, as is often done). With atomic aggregation the model learns atomic energies such that they sum to the total energy. Similarly, with species aggregation the model learns the average energy of each species which in a sum weighted by the number of atoms of each species yields the total energy. Global aggregation amounts to attributing one feature vector to the entire configuration in which case Eq. (1) may be used. Atomic aggregation is equivalent to popular techniques such as GAP, but introduces poor computational scaling as the number of atomic environments in a training set may be very large – generally necessitating the introduction of approximate GPR techniques such as the use of a sparsified GPR, that uses a subset of the data as inducing points to make training feasible and limit prediction time. Finally using *species aggregation* a configuration is described by as many vectors as there are unique atomic species with each vector describing the average environment of that species and  $l_m$  counting the number of atoms of each species. This reduces the computational expense and eliminates the need for approximate GPR techniques while offering improved resolution compared to global aggregation. A similar scheme has previously been used for filtering of atomic structures [36].

We use this species aggregation GPR model in combination with CHGNet in a  $\Delta$ -learning scheme, where the GPR learns to correct the errors of CHGNet, we will refer to this as  $\Delta$ GP-CHGNet for the remainder of the article. A final note on the GPR model, in addition to extracting features from CHGNet we may also leverage the automatic differentiation capabilities of PyTorch that CHGNet is written in. This means derivatives of the total  $\Delta$ GP-CHGNet energy can be computed at essentially no additional expense compared to those of just CHGNet. Additionally, this way of evaluating forces does not require the implementation of any analytical derivatives, be it of features or kernels, which is normally the most challenging and error-prone part of implementing a GPR for the prediction of atomistic properties.

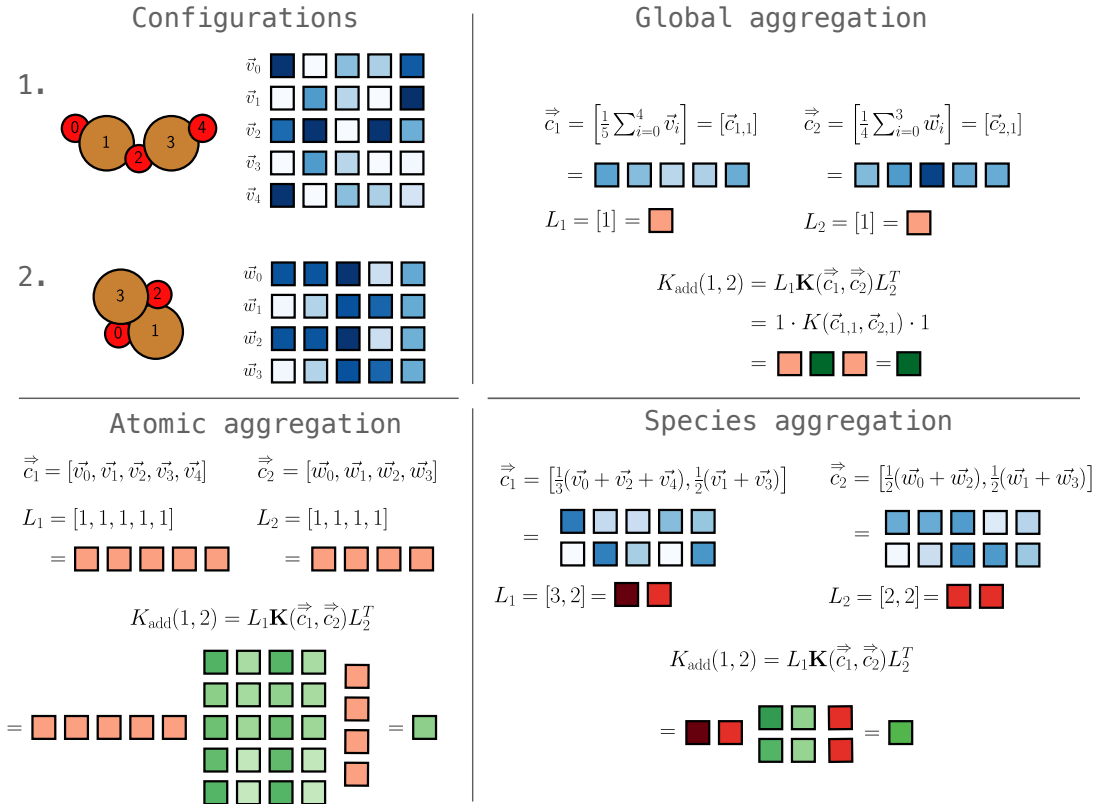


FIG. 2. Illustration of aggregation procedures for two configurations. For *global aggregation* each configuration is represented by a single vector and the additive kernel reduces to a simple kernel between the vectors for each configuration. For *atomic aggregation* each configuration is represented by vectors describing the environment of each atom with unit weight  $L$ . Finally for *species aggregation* each configuration is represented by two vectors each describing the average oxygen and copper, as the first configuration has more oxygen than the second they have different  $L$ .

### C. Global structure search

In the applications of the  $\Delta$ -learning augmented CHGNet model, we will study the stability of surfaces consisting of a fixed slab and an overlayer with variable stoichiometry. To find the optimal geometry for each stoichiometry we employ the GOFEE optimization algorithm as implemented in AGOX [24, 26]. This algorithm iteratively explores the potential energy surface guided by a surrogate model, an outline of each iteration is as follows

1. Create a number of structures.
2. Locally optimize each structure in the lower-confidence bound of the current surrogate model.
3. Select the most promising candidate according to an acquisition function that takes the surrogate prediction into account.
4. Perform a single-point DFT calculation for the selected candidate and store it in a database.
5. Update the surrogate model with the new data point.

We run a number of such searches for each stoichiometry for a fixed number of iterations. This results in a number of configurations with total energies calculated at the DFT level for each stoichiometry. The DFT settings we employed are described in . To establish which stoichiometry/phase is stable under different conditions the Gibbs free energy is calculated as

$$\Delta G = E_T - E_{\text{slab}} - \sum_Z n_Z (\Delta \mu_Z + \varepsilon_Z). \quad (5)$$

Where  $E_T$  is the total energy,  $E_{\text{slab}}$  is the total energy of the clean slab,  $n_Z$  is the number of atoms with atomic number  $Z$  in the overlayer and finally  $\Delta \mu_Z$  and  $\varepsilon_Z$  are the chemical potential and reference energy of atoms with atomic number  $Z$ .

## III. RESULTS

### A. Copper-oxide

The first system we investigate is that of the "8" Cu oxide, which is an ultra-thin oxide film on Cu(111). For

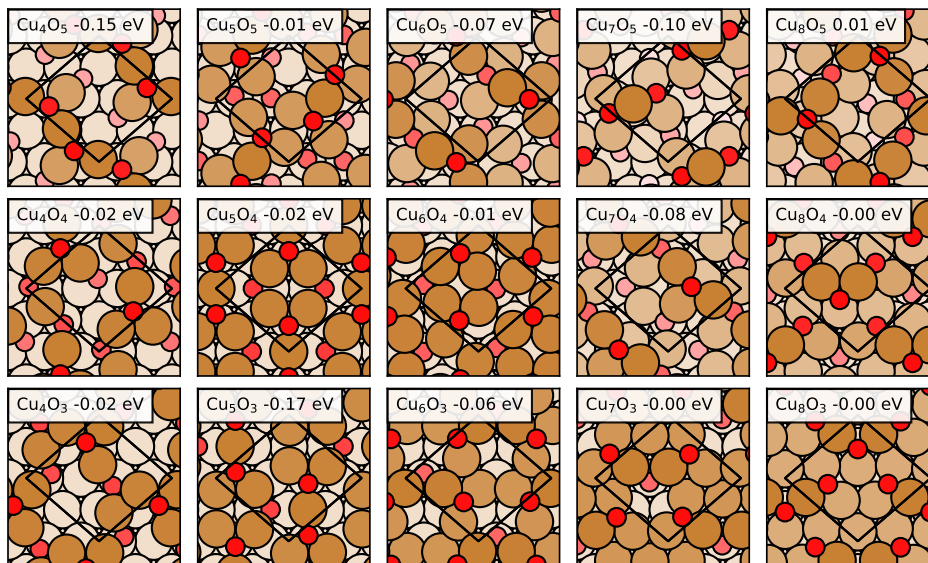


FIG. 3. Minimum energy structures for each stoichiometry found with  $\Delta$ GP-CHGNet, the energies reported in the insets are the difference between the lowest energy structure found when employing a  $\Delta$ -model and those with just CHGNet, both calculated (including relaxations) with DFT. Small and large circles represent Cu and O atoms, respectively. The atoms are colored according to height above the slab with higher atoms being darker in color. The unit cell is shown in black.

this system, LEED shows evidence of a periodic structure forming within a  $c(8 \times 4)$  surface cell, see Ref. 37 and references therein. A structural model containing 8 Cu and 4 O atoms was originally proposed based on the experimental evidence in 2008 by Moritani *et al.*[37]. Recently, the model was revised based on density functional theory calculations by Kim *et al.*[38]. However, no full

phase diagram has been constructed leaving this system open for discovery of new phases.

To supplement the previous studies, we have therefore considered stoichiometries of the ultra-thin oxide film,  $\text{Cu}_x\text{O}_y$ , with  $x = [4, 5, 6, 7, 8]$  and  $y = [3, 4, 5]$ . The reference energy for Cu is calculated as the difference in the total energy of a four and three-layer slab divided by the difference in the number of atoms. The reference energy for oxygen is half of the total energy of an  $\text{O}_2$  molecule from a spin-polarized calculation.

For each stoichiometry we employ the optimization algorithm described in Section II C with CHGNet-v0.3.0 and with  $\Delta$ GP-CHGNet-v0.3.0. The lowest energy structures found by the searches with the  $\Delta$ GP model are reported in Fig. 3. It is evident from this figure that for most stoichiometries the structures found with the  $\Delta$ GP are only slightly more stable than those found by just searching in CHGNet. This shows the remarkable ability of CHGNet to predict new, unpublished, structures for materials solely based on being trained on a wide variety of examples, the vast majority of which are bulk and not surfaces.

The phase diagram for this system is shown in Figure 4. Which shows that for a wide range of chemical potentials for oxygen the preferred phase is  $\text{Cu}_5\text{O}_4$ . We note that by considering a wide range of  $\text{Cu}_x\text{O}_y$  stoichiometries, the present search reveals a new structure that challenges the previous assignment of Kim *et al.* [38], which however is also contained in Fig. 4 as the most stable structure at that given stoichiometry,  $\text{Cu}_8\text{O}_4$ . While LEED-IV studies or surface X-ray diffraction experiments would be required to conclusively discriminate which structural model conforms best with the actual

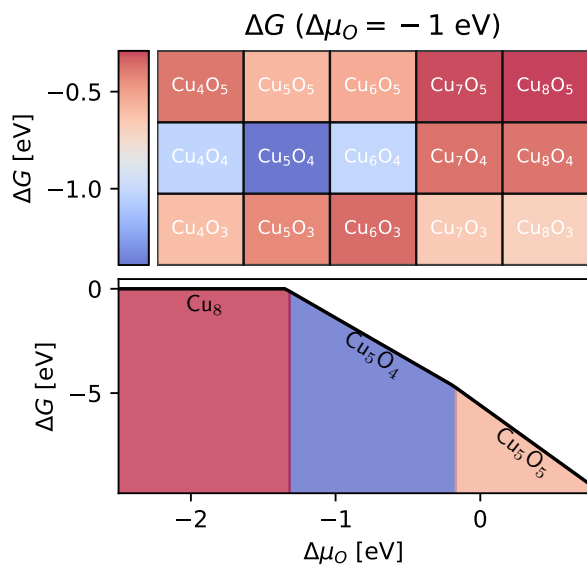


FIG. 4. Top: Raster plot of the Gibbs free energy at  $\Delta\mu_{\text{O}} = -1$  eV. Bottom: Phase diagram showing the most stable phase as a function of the chemical potential of oxygen.

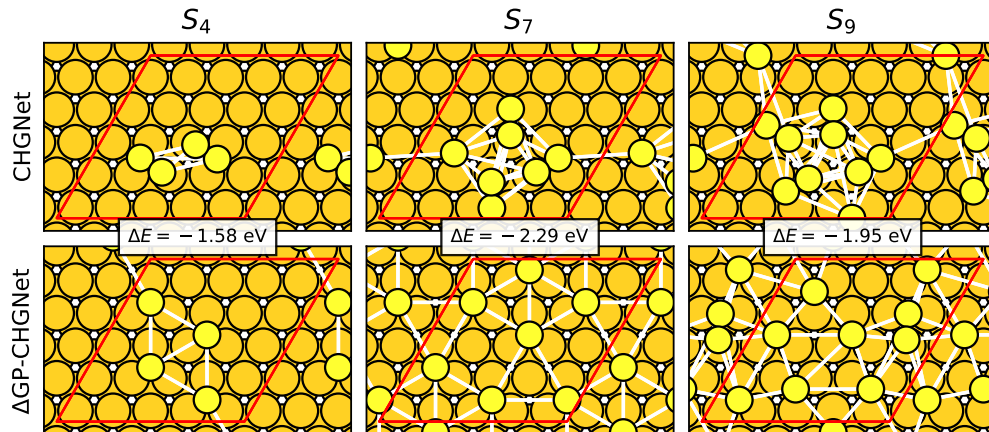


FIG. 5. Most energetically favorable, as evaluated using DFT, structures for three selected values for the number of sulfur atoms found with CHGNet (top) and  $\Delta$ GP-CHGNet (bottom). The energies reported in the top row are calculated as  $\Delta E = E_{\Delta\text{GP-CHGNet}} - E_{\text{CHGNet}}$  where the subscripts indicate the method used to find the configurations but both are evaluated with DFT. The unit cell is shown in red.

Cu "8" oxide, it seems likely that the new  $\text{Cu}_5\text{O}_4$  is the correct structure as this aligns with the findings of an identical structure for  $\text{Ag}(111)$  [39, 40] and a similar non-commensurate structure for  $\text{Pd}(111)$  [41].

### B. Sulfur adsorption on Au(111)

The next system studied is that of sulfur adsorption on Au(111). For this system, an adsorption phase having a  $(5 \times 5)$  super cell has been observed with LEED, see Ref. 42, and a surface structure with 7 sulfur atoms in a 'Rosette' was proposed as the underlying structure. The occurrence of this pattern is attributed to slightly repulsive interactions between adsorbed sulfur atoms. We investigate the efficacy of CHGNet and our proposed  $\Delta$ GP-CHGNet model for structural exploration of this system.

Again, we perform searches using only CHGNet and using  $\Delta$ GP-CHGNet, in Figure 5 the most stable configurations found with the number of sulfur atoms  $N_S = [2, 7, 9]$  for both methodologies is shown. For this system, the differences in stability between structures identified purely with CHGNet and those found with  $\Delta$ GP-CHGNet are very significant. Out of the box CHGNet-v0.3.0 generally prefers sulfur dimers whereas  $\Delta$ GP-CHGNet learns that it is preferential for sulfur atoms to sit in separate hollow-fcc sites. This tendency may be observed in all three stoichiometries depicted in Figure 5. With four sulfur atoms, two dimers are arranged in a small cluster, with seven sulfur atoms three dimers and a lone sulfur atom form a cluster and finally for nine atoms four dimers and a lone sulfur form a cluster. In contrast, for all these structures, DFT prefers separated atoms forming extended overlayers – only forming dimers when the number of sulfur atoms added to the surface is relatively high.

Given the large configurational discrepancies between

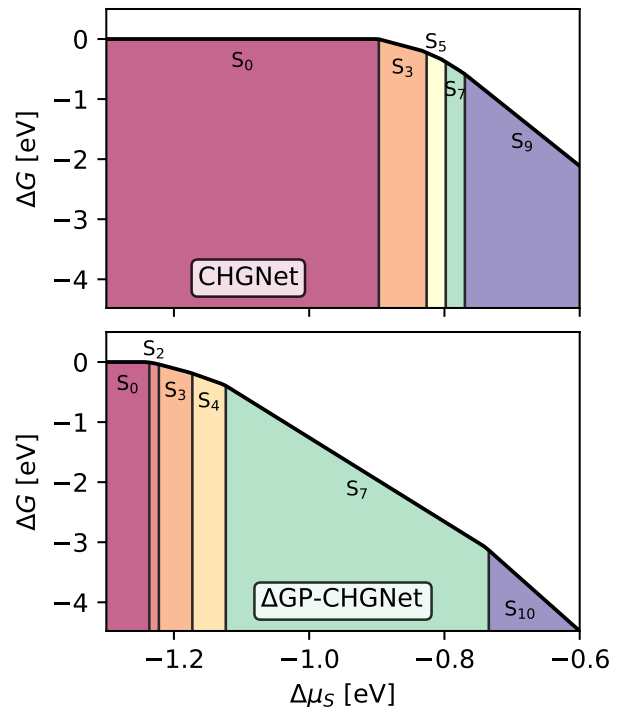


FIG. 6. Predicted Gibbs free energy phase diagrams as a function of the chemical potential of sulfur for structures found using out of the box CHGNet (top) and using  $\Delta$ GP-CHGNet (bottom).

the two search methodologies it is unsurprising that the Gibbs free energy diagrams differ extensively, as is shown in Figure 6. For this system, if relying entirely on CHGNet no phases are predicted correctly except the trivial bare surface for which the chemical potential  $\Delta\mu_S$  necessary for its occurrence is rather inaccurate.

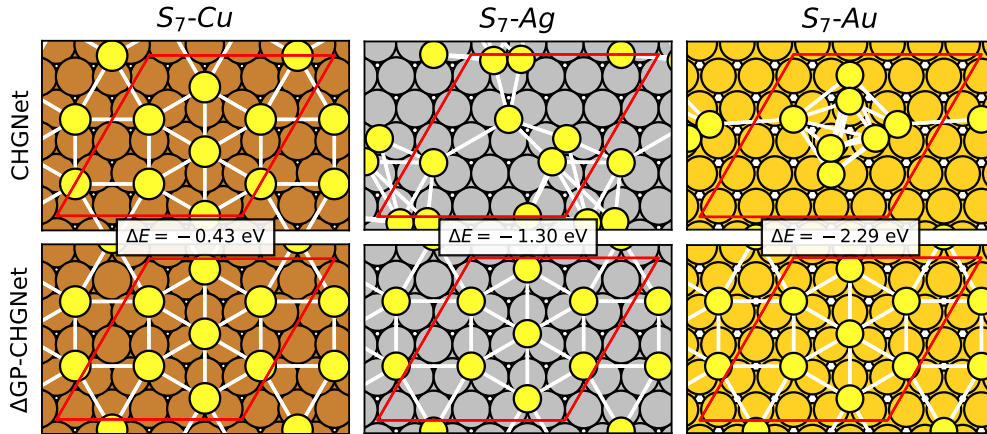


FIG. 7. Sulfur overlayer global minimums identified with CHGNet (top) and  $\Delta$ -GP CHGNet (bottom). The energy difference, with DFT, between the two structures is given. With  $\Delta$ -GP CHGNet the same motif is found for all three metals, whereas without the correction dimers are formed for silver and gold. CHGNet predicts the correct motif on copper, but it is shifted to sulfur on hcp hollow sites.

### C. Analysis

So far, we have seen results for two systems. One where the universal potential CHGNet is able to predict a rather complex surface-oxide structure. However, for the other system the universal potential struggles significantly and consistently favors configurations with an erroneous bonding motif. For other metal-sulfur adsorption structures, such as S/Cu and S/Ag discrepancies between structures preferred in CHGNet and DFT are also present but to a lesser extent. This is illustrated in Fig 7. In fact, for Cu(111)-(5 $\times$ 5)-7S the correct motif is the global minimum of CHGNet, but it is shifted from sulfur sitting on fcc hollow sites to hcp hollow sites. For silver a cluster containing several dimers is the preferred structure according to CHGNet, whereas with DFT the same motif as for gold and copper is obtained.

To facilitate an analysis of the origin of the poor CHGNet description of S/Ag(111) and S/Au(111) systems, we have found it instructive to reduce the complexity of the sulfur structure by studying systems with only two sulfur atoms present in the cell. For all three metals Cu, Ag, and Au it can be found with DFT that configurations in which the two sulfur atoms are separated are more stable than configurations in which they form a dimer on the surface. A full pathway from two separated sulfur atoms to a sulfur dimer can be calculated, see Fig. 8 for an example for the Cu(111) surface.

In an effort to investigate the reasons for this difference in CHGNet’s ability to predict physically realistic results we wish to understand which parts of the Materials Project training data are likely to have influenced the predictions for each system. For this reason, we compute the CHGNet features for every sulfur for various metal-sulfides present in the MPtrj dataset alongside the features of sulfur atoms of the  $S_2$  system for trajectories

starting with the separated sulfur atoms and ending with a sulfur dimer. Such features may be compared using a similarity metric, such as a normalized dot product. For each configuration of the  $S_2$ -trajectories we compute

$$\mathcal{S}(k) = \frac{1}{2N} \sum_i^N \sum_j^2 \frac{\vec{v}_i \cdot \vec{w}_j(k)}{|\vec{v}_i| |\vec{w}_j(k)|} \quad (6)$$

Where  $\vec{v}_i$  is the CHGNet representation of a sulfur-atom in the MPtrj dataset, either from configurations involving both sulfur and metal atoms or from configurations involving only sulfur atoms.  $\vec{w}_j(k)$  is the representation of the  $j$ ’th sulfur atom for configuration  $k$  along the trajectory. The result of this is shown in Fig. 8. On copper the similarity towards sulfur atoms in environments containing both Cu and S remains largely constant along the pathway, while the similarity involving only S increases as the dimer is formed. In contrast, on both silver and gold the similarity towards sulfur atoms in environments containing the metal decreases sharply at the same time as the similarity towards sulfur in environments containing only sulfur increases. That is, for sulfur on silver and gold CHGNet relies too heavily on information gathered from pure sulfur configurations where dimers are very stable. This may explain why CHGNet can identify that on copper the dimer is not preferential, while on silver and gold it is unable to do so – which then leads to erroneous configurations when additional sulfur atoms are introduced.

Further evidence for this explanation is found from the number of sulfur environments originating from configurations of different types present in the MPtrj training dataset, presented in Table I. For  $\text{Cu}_x\text{S}_y$  the number of configurations is comparable to the number of configurations of pure sulfur, whereas for silver and especially for gold the number of configurations and environments is substantially less than those of pure sulfur. It stands to

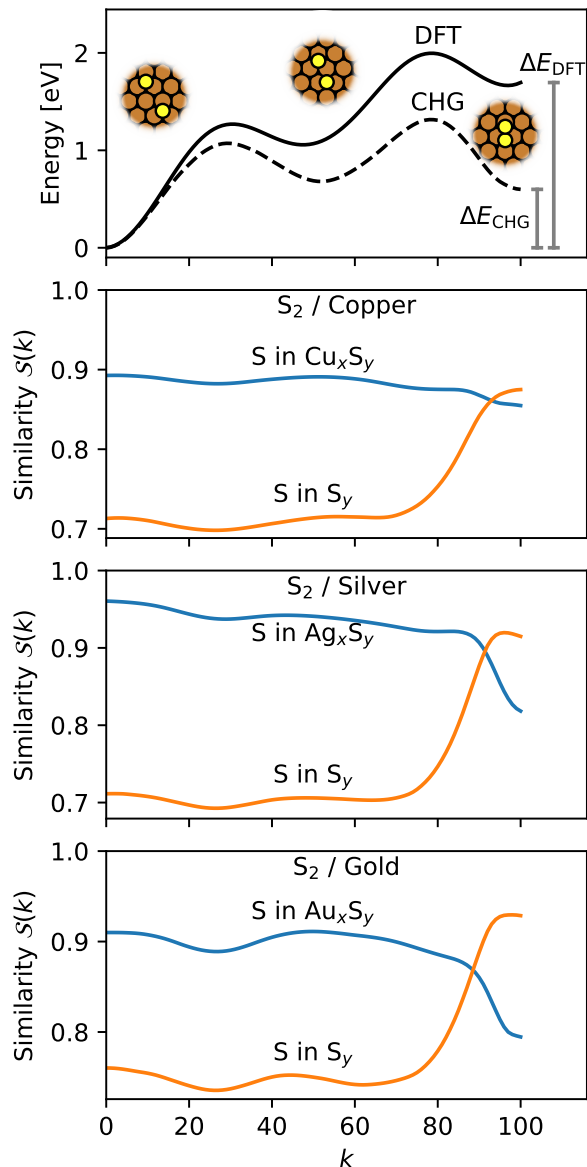


FIG. 8. Energy profiles for combining two sulfur atoms on a copper surface. Average dot product similarity for sulfur atoms for a trajectory starting with separately adsorbed sulfur atoms ending with a  $S_2$ -dimer. The blue lines shows the average similarity against sulfur atoms present in MPTrj in structures of the form  $X_xS_y$  where  $X$  is copper, silver or gold. The orange lines measures the similarity against sulfur atoms from MPTrj in structures containing only sulfur.

reason, that this imbalance has at least partially induced the overreliance on sulfur environments from configurations containing only sulfur.

CHGNet is not the only universal potential trained on MPTrj. In Figure 9 we show the relative stability of  $S_2$  dimers compared to two separated  $S$  atoms on the three different metals calculated with DFT and four machine learning potentials. All of them overestimate the stability of the dimer, but by various amounts and as with

Element	Configurations	Environments
Cu + O	647	3268
Cu + S	548	5154
Ag + S	374	828
Au + S	17	42
S only	636	20450

TABLE I. Number of configurations in MPTrj of the form  $M_xS_y$  for different metals and the number of configurations containing only sulfur along with the total number of sulfur environments for each type of configuration. In addition, the table lists the number of  $Cu_xO_y$  configurations and the number of oxygen environments in those in MPTrj.

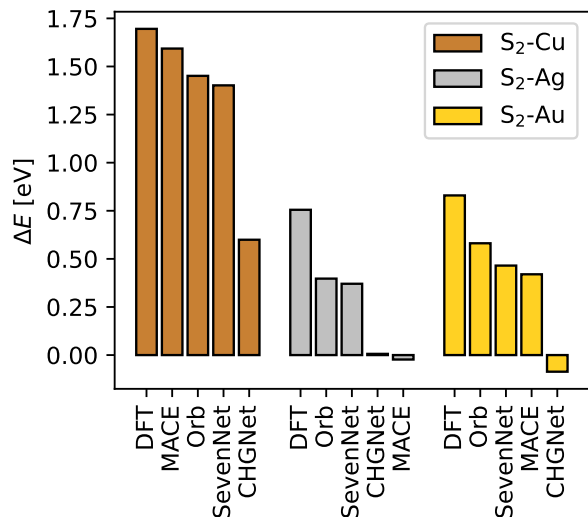


FIG. 9. Relative stability of sulfur-dimer compared to two separated sulfur atoms on copper, silver and gold. Relative stabilities have been calculated using DFT, CHGNet-0.3.0, MACE-MP0, SevenNet-0 and ORB-v2-only-MPTrj – which all are trained on the MPTrj dataset. Positive values indicate that the dimer is less stable than the two separated atoms. A visual representation of these numbers are depicted in Fig. 8(a)

CHGNet the errors are generally smallest when the metal is copper.

#### IV. CONCLUSION

We have investigated the use of a universal potential, CHGNet, for the task of global minimum energy structure prediction, specifically for two systems an oxygen induced surface reconstruction of copper and sulfur overlayers on group 11 metals. Further, we introduce a  $\Delta$ -learning method on top of the universal potential in order to perform global optimization searches with both the out-of-the-box CHGNet and this adapted  $\Delta$ -GP-CHGNet model.

For the "8" Cu surface oxide we find a new global

minimum structure and show that this is a discovery that as-is CHGNet is capable of supporting. Whereas we for the sulfur overlay systems find that CHGNet has flawed understanding that leads to false predictions for the global minimum energy structures. Analyzing the behavior of CHGNet for the  $S_2$  dimer in various metallic embeddings, we traced the origin of the false predictions to CHGNet overestimating the stability of the sulfur-dimer. By inspecting the MPtrj dataset using the representations CHGNet has learned during its training on this dataset, we find that a possible cause for CHGNet's mistaken understanding of adsorbed sulfur dimers is an overreliance on the parts of the training data that only involve sulfur.

Universal potentials provide the materials science community with the opportunity to investigate more and larger systems and allows realistic materials modelling to be done with much fewer computational resources. However, they do not come with guarantees and may, as we have shown, be severely mistaken. Users should be wary and make sure to test the correctness of any such po-

tential, at least for a scaled-down version of their system of interest. Our efforts are one way of adding some explainability to the predictions of a universal potential, further work may involve the application of other model interpretability methods such as TracInCP for the identification of influential training examples [43].

## V. DATA AVAILABILITY

The data and code supporting for this article is openly available from [gitlab.com/agox/agox-chg](https://gitlab.com/agox/agox-chg).

## VI. ACKNOWLEDGEMENTS

We acknowledge support from VILLUM FONDEN through Investigator grant, project no. 16562, and by the Danish National Research Foundation through the Center of Excellence "InterCat" (Grant agreement no: DNR150).

- 
- [1] G. Wang, C. Wang, X. Zhang, Z. Li, J. Zhou, and Z. Sun, *iScience* **27**, 109673 (2024).
- [2] J. Behler and M. Parrinello, *Phys. Rev. Lett.* **98**, 146401 (2007).
- [3] A. P. Bartók, M. C. Payne, R. Kondor, and G. Csányi, *Phys. Rev. Lett.* **104**, 136403 (2010).
- [4] M. Rupp, A. Tkatchenko, K.-R. Müller, and O. A. Von Lilienfeld, *Phys. Rev. Lett.* **108**, 058301 (2012).
- [5] J. Behler, *Int. J. Quantum Chem.* **115**, 1032 (2015).
- [6] V. Botu, R. Batra, J. Chapman, and R. Ramprasad, *J. Phys. Chem. C* **121**, 511 (2017).
- [7] J. Gilmer, S. S. Schoenholz, P. F. Riley, O. Vinyals, and G. E. Dahl, in *Proceedings of the 34th International Conference on Machine Learning*, Proceedings of Machine Learning Research, Vol. 70 (PMLR, 2017).
- [8] K. Schütt, P.-J. Kindermans, H. E. Sauceda Felix, S. Chmiela, A. Tkatchenko, and K.-R. Müller, in *Advances in Neural Information Processing Systems*, Vol. 30, edited by I. Guyon, U. V. Luxburg, S. Bengio, H. Wallach, R. Fergus, S. Vishwanathan, and R. Garnett (Curran Associates, Inc., 2017).
- [9] N. Thomas, T. Smidt, S. Kearnes, L. Yang, L. Li, K. Kohlhoff, and P. Riley, "Tensor field networks: Rotation- and translation-equivariant neural networks for 3D point clouds," (2018), arXiv:1802.08219 [cs].
- [10] B. Anderson, T.-S. Hy, and R. Kondor, "Cormorant: Covariant Molecular Neural Networks," (2019), arXiv:1906.04015 [physics, stat].
- [11] O. T. Unke and M. Meuwly, *J. Chem. Theory Comput.* **15**, 3678 (2019).
- [12] K. Schütt, O. Unke, and M. Gastegger, in *Proceedings of the 38th International Conference on Machine Learning* (PMLR, 2021) pp. 9377–9388.
- [13] V. L. Deringer, A. P. Bartók, N. Bernstein, D. M. Wilkins, M. Ceriotti, and G. Csányi, *Chem. Rev.* **121**, 10073 (2021).
- [14] S. Batzner, A. Musaelian, L. Sun, M. Geiger, J. P. Mailoa, M. Kornbluth, N. Molinari, T. E. Smidt, and B. Kozinsky, *Nat Commun* **13**, 2453 (2022).
- [15] H. Montes-Campos, J. Carrete, S. Bichelmaier, L. M. Varela, and G. K. H. Madsen, *J. Chem. Inf. Model.* **62**, 88 (2022).
- [16] I. Batatia, D. P. Kovacs, G. Simm, C. Ortner, and G. Csányi, in *Advances in Neural Information Processing Systems*, Vol. 35, edited by S. Koyejo, S. Mohamed, A. Agarwal, D. Belgrave, K. Cho, and A. Oh (Curran Associates, Inc., 2022) pp. 11423–11436.
- [17] D. M. Anstine and O. Isayev, *J. Phys. Chem. A* **127**, 2417 (2023).
- [18] B. Deng, P. Zhong, K. Jun, J. Riebesell, K. Han, C. J. Bartel, and G. Ceder, *Nat. Mach. Intell.* **5**, 1031 (2023).
- [19] L. Chanussot, A. Das, S. Goyal, T. Lavril, M. Shuaibi, M. Riviere, K. Tran, J. Heras-Domingo, C. Ho, W. Hu, A. Palizhati, A. Sriram, B. Wood, J. Yoon, D. Parikh, C. L. Zitnick, and Z. Ulissi, *ACS Catal* **11**, 6059 (2021).
- [20] R. Tran, J. Lan, M. Shuaibi, B. M. Wood, S. Goyal, A. Das, J. Heras-Domingo, A. Kolluru, A. Rizvi, N. Shoghi, A. Sriram, F. Therrien, J. Abed, O. Voznyy, E. H. Sargent, Z. Ulissi, and C. L. Zitnick, *ACS Catal* **13**, 3066 (2023).
- [21] I. Batatia, P. Benner, Y. Chiang, A. M. Elena, D. P. Kovács, J. Riebesell, X. R. Advincula, M. Asta, W. J. Baldwin, N. Bernstein, A. Bhowmik, S. M. Blau, V. Cărare, J. P. Darby, S. De, F. D. Pia, V. L. Deringer, R. Elijošius, Z. El-Machachi, E. Fako, A. C. Ferrari, A. Genreith-Schriever, J. George, R. E. A. Goodall, C. P. Grey, S. Han, W. Handley, H. H. Heenen, K. Hermansson, C. Holm, J. Jaafar, S. Hofmann, K. S. Jakob, H. Jung, V. Kapil, A. D. Kaplan, N. Karimitari, N. Kroupa, J. Kullgren, M. C. Kuner, D. Kuryła, G. Liepuoniute, J. T. Margraf, I.-B. Magdău, A. Michaelides, J. H. Moore, A. A. Naik,

- S. P. Niblett, S. W. Norwood, N. O'Neill, C. Ortner, K. A. Persson, K. Reuter, A. S. Rosen, L. L. Schaaf, C. Schran, E. Sivonxay, T. K. Stenczel, V. Svahn, C. Sutton, C. van der Oord, E. Varga-Umbrich, T. Vegge, M. Vondrák, Y. Wang, W. C. Witt, F. Zills, and G. Csányi, (2023), arXiv:2401.00096 [physics.chem-ph].
- [22] J. Kim, J. Kim, J. Kim, J. Lee, Y. Park, Y. Kang, and S. Han, *J. Am. Chem. Soc.* **147**, 1042 (2024).
- [23] M. Neumann, J. Gin, B. Rhodes, S. Bennett, Z. Li, H. Choubisa, A. Hussey, and J. Godwin, "Orb: A Fast, Scalable Neural Network Potential," (2024), arXiv:2410.22570 [cond-mat].
- [24] M. K. Bisbo and B. Hammer, *Phys. Rev. Lett.* **124**, 086102 (2020).
- [25] J. Timmermann, F. Kraushofer, N. Resch, P. Li, Y. Wang, Z. Mao, M. Riva, Y. Lee, C. Staacke, M. Schmid, C. Scheurer, G. S. Parkinson, U. Diebold, and K. Reuter, *Phys. Rev. Lett.* **125**, 206101 (2020).
- [26] M.-P. V. Christiansen, N. Rønne, and B. Hammer, *J. Chem. Phys.* **157**, 054701 (2022).
- [27] D. Chen, C. Shang, and Z.-P. Liu, *J. Chem. Phys.* **156**, 094104 (2022).
- [28] C. Larsen, S. Kaappa, A. L. Vishart, T. Bligaard, and K. W. Jacobsen, *Phys. Rev. B* **107**, 214101 (2023).
- [29] P. Lyngby, C. Larsen, and K. W. Jacobsen, *Physical Review Materials* **8**, 123802 (2024).
- [30] J. Pitfield, F. Brix, Z. Tang, A. M. Slavensky, N. Rønne, M.-P. V. Christiansen, and B. Hammer, *Phys. Rev. Lett.* **134**, 056201 (2025).
- [31] J. Behler, *J. Chem. Phys.* **134**, 074106 (2011).
- [32] A. R. Oganov and M. Valle, *J. Chem. Phys.* **130**, 104504 (2009).
- [33] A. P. Bartók, R. Kondor, and G. Csányi, *Phys. Rev. B* **87**, 184115 (2013).
- [34] K. Schütt, O. Unke, and M. Gastegger, in *Proceedings of the 38th International Conference on Machine Learning*, Proceedings of Machine Learning Research, Vol. 139, edited by M. Meila and T. Zhang (PMLR, 2021) pp. 9377–9388.
- [35] S. Batzner, A. Musaelian, L. Sun, M. Geiger, J. P. Mailoa, M. Kornbluth, N. Molinari, T. E. Smidt, and B. Kozinsky, *Nat Commun* **13**, 2453 (2022).
- [36] P. Kovács, E. Heid, J. De Landsheere, and G. K. H. Madsen, "LoGAN: Local generative adversarial network for novel structure prediction," (2024).
- [37] K. Moritani, M. Okada, Y. Teraoka, A. Yoshigoe, and T. Kasai, *J. Phys. Chem. C* **112**, 8662 (2008).
- [38] H. J. Kim, G. Lee, S.-H. V. Oh, C. Stampfl, and A. Soon, *ACS Nano* **18**, 4559 (2024).
- [39] J. Schnadt, J. Knudsen, X. L. Hu, A. Michaelides, R. T. Vang, K. Reuter, Z. Li, E. Lægsgaard, M. Scheffler, and F. Besenbacher, *Phys. Rev. B* **80**, 075424 (2009).
- [40] H. L. Mortensen, S. A. Meldgaard, M. K. Bisbo, M.-P. V. Christiansen, and B. Hammer, *Physical Review B* **102**, 075427 (2020).
- [41] E. Lundgren, G. Kresse, C. Klein, M. Borg, J. N. Andersen, M. De Santis, Y. Gauthier, C. Konvicka, M. Schmid, and P. Varga, *Phys. Rev. Lett.* **88**, 246103 (2002).
- [42] M. Yu, H. Ascolani, G. Zampieri, D. P. Woodruff, C. J. Satterley, R. G. Jones, and V. R. Dhanak, *J. Phys. Chem. C* **111**, 10904 (2007).
- [43] G. Pruthi, F. Liu, S. Kale, and M. Sundararajan, in *Advances in Neural Information Processing Systems*, Vol. 33 (Curran Associates, Inc., 2020) pp. 19920–19930.
- [44] A. Hjorth Larsen, J. Jørgen Mortensen, J. Blomqvist, I. E. Castelli, R. Christensen, M. Dułak, J. Friis, M. N. Groves, B. Hammer, C. Hargus, E. D. Hermes, P. C. Jennings, P. Bjerre Jensen, J. Kermode, J. R. Kitchin, E. Leonhard Kolsbjerg, J. Kubal, K. Kaasbjerg, S. Lysgaard, J. Bergmann Maronsson, T. Maxson, T. Olsen, L. Pastewka, A. Peterson, C. Rostgaard, J. Schiøtz, O. Schütt, M. Strange, K. S. Thygesen, T. Vegge, L. Vilhelmsen, M. Walter, Z. Zeng, and K. W. Jacobsen, *J. Phys. Condens. Matter* **29**, 273002 (2017).
- [45] J. J. Mortensen, A. H. Larsen, M. Kuisma, A. V. Ivanov, A. Taghizadeh, A. Peterson, A. Haldar, A. O. Dohn, C. Schäfer, E. Ö. Jónsson, E. D. Hermes, F. A. Nilsson, G. Kastlunger, G. Levi, H. Jónsson, H. Häkkinen, J. Fojt, J. Kangsabanik, J. Sødequist, J. Lehtomäki, J. Heske, J. Enkovaara, K. T. Winther, M. Dulak, M. M. Melander, M. Ovesen, M. Louhivuori, M. Walter, M. Gjerding, O. Lopez-Acevedo, P. Erhart, R. Warmbier, R. Würdemann, S. Kaappa, S. Latini, T. M. Boland, T. Bligaard, T. Skovhus, T. Susi, T. Maxson, T. Rossi, X. Chen, Y. L. A. Schmerwitz, J. Schiøtz, T. Olsen, K. W. Jacobsen, and K. S. Thygesen, *J. Chem. Phys.* **160**, 092503 (2024).

## Appendix A: Appendix: DFT Settings

All DFT calculations have been performed with the GPAW code [44, 45]. For copper-oxide a plane-wave cutoff of 400 eV was used, a (4×4) Monkhorst-Pack k-point grid, with the PBE exchange-correlation functional. For the metal-sulfides we employed a cutoff of 520 eV and Monkhorst Pack grids with a density of 3.5 points/Å<sup>-1</sup> again with the PBE functional.